


# Acetyltransferase GCN5 regulates autophagy and lysosome biogenesis by targeting TFEB

Yusha Wang<sup>1</sup>, Yewei Huang<sup>1</sup>, Jiaqi Liu<sup>1</sup>, Jinna Zhang<sup>1</sup>, Mingming Xu<sup>1</sup>, Zhiyuan You<sup>1</sup>, Chao Peng<sup>2</sup>, Zhefeng Gong<sup>3</sup> & Wei Liu<sup>1,4,\*</sup> 

## Abstract

Accumulating evidence highlights the role of histone acetyltransferase GCN5 in the regulation of cell metabolism in metazoans. Here, we report that GCN5 is a negative regulator of autophagy, a lysosome-dependent catabolic mechanism. In animal cells and *Drosophila*, GCN5 inhibits the biogenesis of autophagosomes and lysosomes by targeting TFEB, the master transcription factor for autophagy- and lysosome-related gene expression. We show that GCN5 is a specific TFEB acetyltransferase, and acetylation by GCN5 results in the decrease in TFEB transcriptional activity. Induction of autophagy inactivates GCN5, accompanied by reduced TFEB acetylation and increased lysosome formation. We further demonstrate that acetylation at K274 and K279 disrupts the dimerization of TFEB and the binding of TFEB to its target gene promoters. In a Tau-based neurodegenerative *Drosophila* model, deletion of dGcn5 improves the clearance of Tau protein aggregates and ameliorates the neurodegenerative phenotypes. Together, our results reveal GCN5 as a novel conserved TFEB regulator, and the regulatory mechanisms may be involved in autophagy- and lysosome-related physiological and pathological processes.

**Keywords** acetylation; autophagy; GCN5; lysosome; TFEB

**Subject Categories** Autophagy & Cell Death; Post-translational Modifications & Proteolysis

**DOI** 10.15252/embr.201948335 | Received 22 April 2019 | Revised 4 October 2019 | Accepted 28 October 2019 | Published online 21 November 2019

**EMBO Reports (2020) 21: e48335**

## Introduction

Autophagy is a major cellular turnover pathway whereby intracellular contents are delivered by double-membraned autophagosomes to lysosomes for degradation. While the basal constitutive autophagy serves to clear undesired cellular substances, cells initiate adaptive autophagy in response to intracellular and extracellular cues such as nutrient limitation, DNA damage, and oxidative stress

[1]. Therefore, autophagy plays a dual role of cell metabolism regulation and intracellular quality control, and increasing evidence suggests that dysfunctional autophagy is involved in many pathological processes, such as cancer and neurodegenerative disease [2].

The implementation of autophagy and sustained autophagy flux requires adequate lysosomal activity. Therefore, autophagy is intimately associated with the biogenesis and activation of lysosomes. The role of transcription factor EB (TFEB) is important in this process, on account of the fact that it simultaneously regulates the expression of genes for autophagosome formation and lysosome production [3,4]. As a member of the MiT/TFE family of transcription factors, the activity of TFEB is mainly regulated by mechanistic target of rapamycin (mTOR), which determines the subcellular localizations of TFEB. Phosphorylation of TFEB by mTOR binds TFEB to 14-3-3 protein and retains it in the cytoplasm [5,6], while inactivation of mTOR and/or activation of the phosphatase calcineurin results in dephosphorylated TFEB, which enters nucleus [7]. In addition to mTOR, protein kinase C, glycogen synthase kinase, and Rac- $\alpha$  serine/threonine protein kinase can also phosphorylate TFEB and regulate its translocation from cytoplasm to nucleus [8–10]. Interestingly, recent studies have shown that the transcriptional activity of TFEB is also regulated by its acetylation, and the deacetylation of TFEB significantly improves autophagy and lysosomal function [11]. This suggests that the intracellular acetylation/deacetylation system can not only directly target autophagy-related proteins [12–15], but also directly regulate autophagy at the transcriptional level. Although acetyl-coenzyme A acetyltransferase 1 (ACAT1) and the histone deacetylases SIRT1 and HDAC2 have been reported to affect the acetylation of TFEB [11,16], the molecular mechanism by which acetylation regulates TFEB activity remains unclear.

General control non-repressed protein 5 (GCN5) was initially identified as a histone acetyltransferase in *Tetrahymena* [17,18]. Like other acetyltransferases, besides targeting core histones, GCN5 also exerts its gene regulatory function through acetylation of sequence-specific transcription factors [19–22]. This enables it to participate in a wide range of cellular processes, including cell proliferation, differentiation, telomere maintenance, and DNA

1 Department of Biochemistry and Department of Cardiology of the Second Affiliated Hospital, Zhejiang University School of Medicine, Hangzhou, China

2 National Center for Protein Science Shanghai, Institute of Biochemistry and Cell Biology, Shanghai Institutes of Biological Sciences, Chinese Academy of Sciences, Shanghai, China

3 Department of Neurobiology, Key Laboratory of Medical Neurobiology of the Ministry of Health of China, Zhejiang University School of Medicine, Hangzhou, China

4 Collaborative Innovation Center for Diagnosis and Treatment of Infectious Disease, First Affiliated Hospital, Zhejiang University School of Medicine, Hangzhou, China

\*Corresponding author. Tel: +86 5718 8208357; E-mail: liuwei666@zju.edu.cn

damage repair [20,23–25]. Intriguingly, recent studies have shown that GCN5 is an important regulator of cell metabolism. GCN5 acetylates and inactivates peroxisome proliferator-activated receptor  $\gamma$  coactivator-1 $\alpha$  (PGC-1 $\alpha$ ), thereby regulating the expression of many genes required by various cellular metabolic pathways, including fatty acid oxidation and gluconeogenesis [19,26]. In addition to being activated by its coenzyme acetyl-CoA, the acetyltransferase activity of GCN5 can also be up-regulated by the essential amino acid methionine and insulin–GSK3 $\beta$  signals [27–29]. Animal models showed that the expression of GCN5 is increased by a high-fat diet and decreased by fasting [22,30]. All these results indicate a role for GCN5 in cell energy homeostasis. However, the function of GCN5 in autophagy, a key process of cell catabolism, is still unknown.

In this study, we have determined that GCN5 functions as an inhibitor of autophagy and lysosomal biogenesis in mammalian cells and *Drosophila*. Mechanistically, GCN5 acetylates TFEB, which disturbs the dimerization of TFEB and subsequently the binding of TFEB to its target gene promoters. Silencing GCN5 in a Tau-based *Drosophila* neurodegeneration model ameliorates the neurodegenerative phenotypes by facilitating the elimination of Tau protein aggregates.

## Results

### GCN5 negatively regulates autophagy

To assess the potential role of GCN5 in the regulation of autophagy, we generated GCN5 knockout (GCN5 KO) HeLa and HEK293 cell lines using the CRISPR/Cas9 system. In these cells, an increase in the number of LC3 puncta and the protein level of LC3-II was detected (Figs 1A, B and E, and EV1A–C). The same results were obtained from cells treated with a specific GCN5 inhibitor,  $\alpha$ -methylene- $\gamma$ -butyrolactone 3 (MB-3) (Figs 1C and EV1D and E). Transfection in GCN5 KO cells of wild-type (WT) GCN5 but not the acetyltransferase-defective GCN5-E575Q mutant [31,32] eliminated the increase in LC3 puncta (Fig 1D and E). Furthermore, overexpression of GFP-GCN5 reduced LC3 puncta and LC3-II in WT HeLa cells that show a high level of basal autophagy (Figs 1F–H and EV1F). These data thus suggest an inhibitory effect of GCN5 on autophagosome formation. To evaluate autophagic degradation, we

checked the expression of *SQSTM1/p62*, an autophagy adaptor that is degraded by autophagy. Unexpectedly, in GCN5 KO cells, compared with WT cells, we detected an increase in the level of p62 mRNA, but no significant change in the level of p62 protein (Fig EV1G and H), which suggests that GCN5 inhibited p62 transcription. We then checked the degradation of exogenous GFP-p62, whose transcription is TFEB-independent, in HEK293 cells stably expressing GFP-p62. GCN5 knockdown or MB-3 treatment clearly reduced the GFP-p62 protein in the cells, and this decrease could be blocked by the lysosome inhibitor chloroquine (CQ) (Figs 1I and EV1I and J), which suggests that GCN5 inhibited autophagic degradation. To further confirm this, we examined the expression of IFT20 and PDLIM1 proteins, which are also particularly dependent on autophagy for degradation in cells [33,34]. As expected, the deletion of GCN5 reduced the levels of IFT20 and PDLIM1 in cells, and the transfection of GCN5 into GCN5-deleted cells restored their levels (Figs 1J and EV1K and L).

To obtain evidence that GCN5 inhibits autophagy *in vivo*, we evaluated autophagosome formation in mCherry-Atg8a (homologue of human MAP1LC3/LC3) transgenic *Drosophila* by regulating the expression of dGcn5, the only GCN5 in *Drosophila* [35]. Under feeding conditions, mCherry-Atg8a was diffusely localized in the fat body of *Drosophila* larvae, and neither dGcn5 overexpression nor dGcn5 knockdown had a significant effect on this localization (Fig 1K). However, knocking down dGcn5 significantly promoted the formation of mCherry-Atg8a puncta in starved *Drosophila* larvae, while overexpression of dGcn5 attenuated the formation of puncta (Fig 1K). Taken together, these data suggest that GCN5 is an inhibitor of autophagy.

### GCN5 inhibits lysosomal biogenesis

In GCN5 KO cells, we also observed an increase in the number of lysosomes indicated by lysosome-associated membrane glycoprotein 1 (LAMP1)-positive and LysoTracker-labeled punctate structures (Figs 2A, B and E, and EV2A), accompanied by an increase in the expression of lysosomal proteins including LAMP1 and mature cathepsin D (CTSD) (Figs 2C and EV2B and C). Transfection in the cells of WT GCN5 but not the GCN5-E575Q abolished the increase in lysosome number (Fig 2D and E). In addition, the activity of the lysosomal enzyme  $\beta$ -hexosaminidase increased significantly in these cells (Fig 2F). To further verify the increase in lysosomal activity in

**Figure 1. GCN5 negatively regulates autophagy.**

- A LC3 punctum formation in WT and GCN5 KO HeLa cells (Scale bars, 10  $\mu$ m).
- B, C Immunoblot showing LC3-II formation in WT or GCN5 KO or MB-3-treated HeLa cells in the presence or absence of the lysosome inhibitor Baf.
- D Formation of LC3 puncta in GCN5 KO HeLa cells overexpressing Myc-tagged GCN5 or GCN5-E575Q (Scale bars, 10  $\mu$ m).
- E Quantification of LC3 puncta in cells shown in (A) and (D). The cells were treated with or without Baf (graph represents data from three independent experiments with  $\geq 30$  cells per condition; mean  $\pm$  SEM; \*\*\* $P < 0.001$ , Student's *t*-test).
- F, G Formation of LC3 puncta in HeLa cells overexpressing GFP-GCN5 with or without Baf treatment (graph represents data from three independent experiments with  $\geq 30$  cells per condition; mean  $\pm$  SEM; \* $P < 0.05$ , \*\* $P < 0.01$ , Student's *t*-test; Scale bar, 10  $\mu$ m).
- H LC3-II formation in GFP-GCN5-overexpressing HeLa cells.
- I GFP-p62 levels in HEK293 cells stably expressing GFP-p62. The cells were cultured with GCN5 siRNA with or without CQ.
- J PDLIM1 and IFT20 protein levels in GCN5 KO HEK293 cells with or without transfection of GFP-GCN5 and addition of CQ.
- K Representative images of mCherry-Atg8a (red) and DAPI (blue) in *Drosophila* larval fat body in which dGcn5 is overexpressed (OE) or silenced (KD) using the pan-fat body driver (cg-GAL4). *Drosophila* (cg-GAL4/+) was used as the control (graph represents data from three independent experiments with  $\geq 30$  cells per condition; mean  $\pm$  SEM; \* $P < 0.05$ , \*\*\* $P < 0.001$ , Student's *t*-test; Scale bars, 10  $\mu$ m).

Source data are available online for this figure.

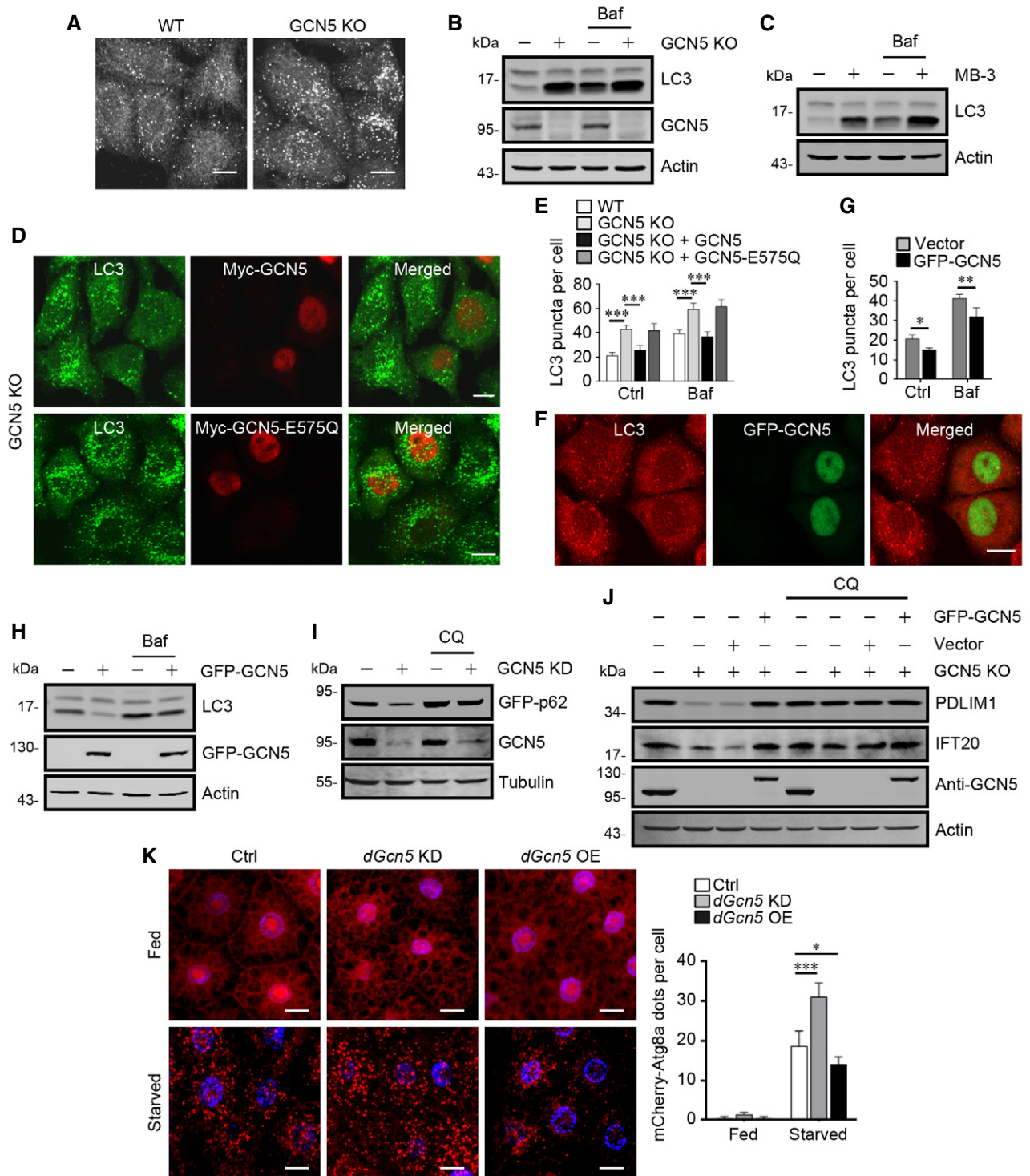
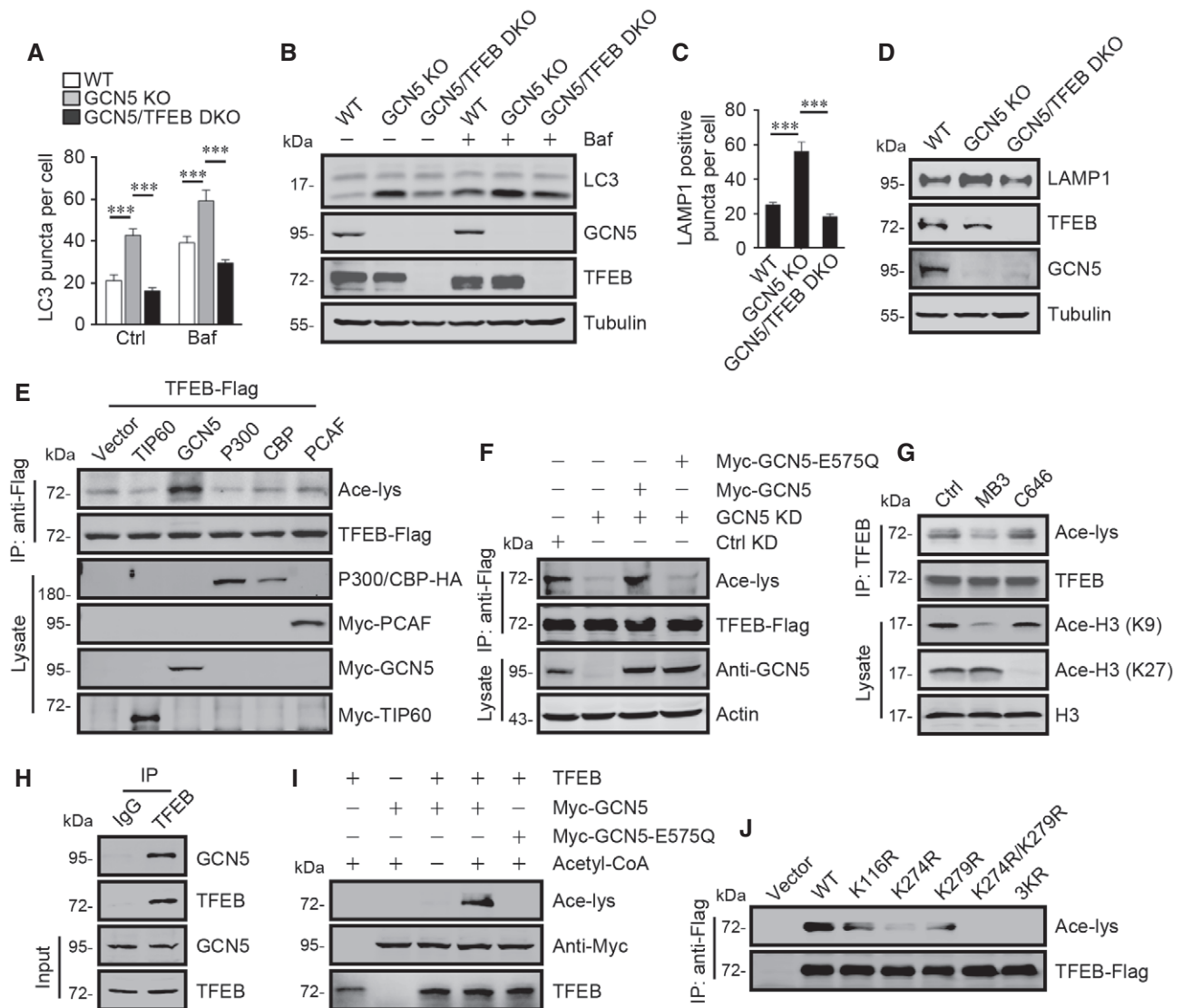


Figure 1.

the cells, we analyzed the processing of epidermal growth factor receptor (EGFR). The absence of GCN5 obviously accelerated EGFR degradation in EGF-stimulated cells (Figs 2G and EV2D). Finally, we assessed the role of GCN5 in lysosomal biogenesis in *Drosophila*. Under feeding conditions, consistent with previous observations [36], LysoTracker marked a few spots in the fat body of *Drosophila*

larvae. The deletion of dGcn5 significantly increased the abundance of LysoTracker-positive punctate structures (Fig 2H). In addition, deletion of dGcn5 further promoted the starvation-stimulated formation of LysoTracker puncta, while overexpression of dGcn5 reduced their formation (Fig 2H). Together, these results suggest that GCN5 is an inhibitor of lysosomal biogenesis.





**Figure 3. GCN5 acetylates TFEB at K116, K274, and K279.**

- A** Quantification of LC3 puncta in WT, GCN5 KO, and GCN5/TFEB DKO HeLa cells in the presence or absence of Baf (graph represents data from three independent experiments with  $\geq 30$  cells per condition; mean  $\pm$  SEM; \*\*\* $P < 0.001$ , Student's *t*-test).
- B** Immunoblot showing LC3-II formation in WT, GCN5 KO, and GCN5/TFEB DKO HeLa cells in the presence or absence of Baf.
- C** Quantification of LAMP1 puncta in WT, GCN5 KO, and GCN5/TFEB DKO HEK293 cells (graph represents data from three independent experiments with  $\geq 30$  cells per condition; mean  $\pm$  SEM; \*\*\* $P < 0.001$ , Student's *t*-test).
- D** Immunoblot showing LAMP1 levels in WT, GCN5 KO, and GCN5/TFEB DKO HEK293 cells.
- E** Acetylation of TFEB-Flag in stable TFEB-Flag-expressing HEK293 cells with overexpression of individual histone acetyltransferases as indicated. TFEB-Flag was immunoprecipitated with anti-Flag beads and analyzed by immunoblot using anti-acetyl-lysine (Ace-lys).
- F** TFEB-Flag acetylation in the stable TFEB-Flag-expressing HEK293 cells transfected with Myc-tagged GCN5 or GCN5-E575Q after incubation with GCN5 siRNA for 48 h.
- G** Acetylation of endogenous TFEB in MEF cells treated with the GCN5 inhibitor MB-3 or the p300/CBP inhibitor C646. H3, histone H3. Ace-H3 (K9) and Ace-H3 (K27) were used to show the activity of GCN5 and p300, respectively.
- H** Co-precipitation of GCN5 with TFEB. TFEB was immunoprecipitated from MEF cells using anti-TFEB, and the precipitates were analyzed using anti-GCN5.
- I** *In vitro* acetylation assays of TFEB. Purified recombinant TFEB was incubated with Myc-GCN5 or Myc-GCN5-E575Q immunoprecipitated from HEK293 cells.
- J** Acetylation of Flag-tagged TFEB or TFEB mutants expressed in HEK293 cells. 3KR: Lys 116, Lys 274, and Lys 279 were replaced by Arg.

Source data are available online for this figure.

### GCN5 acetylates TFEB at K116, K274, and K279

The effect of GCN5 on autophagosome formation, lysosomal biogenesis, and p62 transcription suggests a potential role of GCN5 in

regulating TFEB. To clarify this, we first generated GCN5 and TFEB double knockout cells based on the GCN5 KO cell line and found that deletion of TFEB completely eliminated the increase in LC3-puncta, LC3-II level, and lysosome number induced by GCN5 KO

(Fig 3A–D). We then determined that the intracellular protein level of TFEB remained unchanged when GCN5 was deleted or overexpressed (Fig EV3A). Then, we examined the acetylation of TFEB in cells ectopically expressing GCN5 or the other known autophagy-related acetyltransferases (Fig 3E). Surprisingly, increased acetylation of TFEB was observed only in GCN5-transfected cells (Figs 3E and EV3B), which indicates a specific role of GCN5. In line with this, knockdown of GCN5 reduced the acetylation of TFEB-Flag in cells stably expressing TFEB-Flag, and this reduction was eliminated by introducing WT GCN5 but not GCN5-E575Q (Figs 3F and EV3C). Treatment of cells with the GCN5 inhibitor MB-3 but not the p300 inhibitor C646 also suppressed the acetylation of endogenous TFEB (Figs 3G and EV3D). We then proceeded to determine whether GCN5 directly acetylates TFEB. Firstly, we observed co-immunoprecipitation of GCN5 with TFEB, which indicates an interaction between GCN5 and TFEB (Fig 3H). We then performed an *in vitro* acetylation assay by incubating recombinant TFEB purified from *E. coli* with Myc-GCN5 immunoprecipitated from transfected HEK293 cells. In the presence of acetyl-CoA, we detected marked TFEB acetylation by GCN5-WT but not by GCN5-E575Q (Fig 3I). These data strongly indicate that TFEB is an acetylation substrate of GCN5.

To identify the acetylation sites on TFEB, we analyzed the *in vitro* acetylated TFEB by mass spectrometry. This suggested three potential acetylated residues, K116, K274, and K279 (Fig EV3E–G), among which K116 has been previously reported [11,16]. To verify these acetylation sites, Flag-tagged acetylation-defective TFEB mutants, in which each of the three lysine residues was changed to arginine via site-directed mutagenesis, were constructed and transfected into HEK293 cells. Acetylation assessment confirmed that, in addition to the known K116 in the N-terminal region, K274 and K279 in the bHLH domain of TFEB are novel sites for acetylation by GCN5 (Figs 3J and EV3H).

Compared with K116, which only exists in human TFEB, K274 and K279 are well-conserved in metazoans (Fig EV3I). The corresponding sites in dMitf, the only TFEB in *Drosophila* [37], are K445 and K450 (Fig EV3I). Using gene overexpression and gene knockdown/rescue experiments in *Drosophila* S2 cells, we proved that dGcn5 has acetyltransferase activity toward dMitf, and K445 and K450 on dMitf are the major acetylation sites (Fig EV3J and K).

### Acetylation by GCN5 suppresses TFEB transcriptional activity

To test the potential impact of GCN5-mediated acetylation on the transcriptional activity of TFEB, we first examined the expression of TFEB target genes. In GCN5 KO HEK293 cells, the mRNA levels of autophagy-related *SQSTM1* and *WIP1* and lysosome-related *LAMP1* and *CTSD* increased (Fig 4A). This increase in the genes expressions was completely blocked by depleting TFEB in the cells, suggesting that it depends on TFEB (Fig 4A). Accordingly, knockdown of dGcn5 in *Drosophila* increased the expression of dMitf target genes in larval fat body (Fig 4B). Overexpression of TFEB enhanced the expression of its target genes, and overexpression of the K116R/K274R/K279R (3KR) mutant resulted in an even stronger promotion (Fig 4C). Furthermore, we checked the activity of the promoter of TFEB target genes. Using a luciferase reporter carrying TFEB-binding sites (CLEAR element) [3], we found that GCN5 KO cells (Fig 4D) and TFEB-3KR-overexpressing cells

(Fig 4E) showed higher luciferase activity than WT cells and TFEB-WT-transfected cells, respectively, while TFEB depletion prevented the effect of GCN5 KO (Fig 4D). Together, these results suggested that GCN5-mediated acetylation inhibits the transcriptional activity of TFEB.

### Acetylation disrupts the dimerization and DNA-binding activity of TFEB

To investigate the molecular mechanism underlying the acetylation-mediated inactivation of TFEB, we checked the effect of GCN5 on the intracellular localization of TFEB, which is directly related to TFEB transcriptional activity and is mainly regulated by mTORC1. We noted that deletion of GCN5 affected neither the dominant cytoplasmic distribution of TFEB under basal conditions nor the nuclear accumulation of TFEB after treatment with the mTOR inhibitor Torin1 (Figs 5A and EV4A). In addition, deletion or inhibition of GCN5 showed no effect on mTORC1 activity, as indicated by unchanged the phosphorylation of mTORC1 substrate 4E-BP1 (Fig EV4B). Next, we used the TFEB-S211A mutant, which has prominent nuclear localization [6], as a positive control to explore the function of acetylation on TFEB localization. Both the GCN5 acetylation-defective TFEB-3KR and the acetylation-mimetic TFEB-3KQ, in which the three lysines at the acetylation sites by GCN5 were changed to glutamine, remained in the cytoplasm and transferred normally into the nucleus when the cells were treated with Torin1 (Figs 5B and EV4C). These results suggest that GCN5-dependent acetylation does not affect the intracellular distribution of TFEB. These data therefore support the view that GCN5, which is predominantly localized in the nucleus [19,38], regulates intracellular TFEB activity mainly by targeting the nuclear pool of TFEB. In fact, with cell fractionation, we found both in TFEB-Flag-expressing cells and in WT cells that a small proportion of TFEB-Flag and endogenous TFEB was present in the nucleus even in basal fed culture, which did not depend on their acetylation (Fig EV4D–F). In addition, compared with cytoplasmic TFEB, nuclear TFEB showed a much higher acetylation level, which was strongly inhibited by the treatment of cells with GCN5 inhibitor MB-3 (Fig EV4G). We then performed a chromatin immunoprecipitation (ChIP) assay to detect a potential effect of GCN5-mediated acetylation on the binding of TFEB to its target gene promoters. Intriguingly, compared with WT TFEB, TFEB-3KR showed stronger binding to the promoters of the TFEB target genes *CLCN7*, *GLA*, and *CTSD* in cells, whereas TFEB-3KQ did the opposite (Fig 5C). This was mainly attributed to deacetylation at K274 and K279, because the TFEB-K274R/K279R mutant exhibited similar binding capacity to TFEB-3KR, while the binding of the TFEB-K116R mutant was similar to that of TFEB-WT (Fig 5C). We further carried out *in vitro* electrophoretic mobility shift assays (EMSA) in which purified recombinant TFEB or the TFEB mutants were incubated with a DNA fragment containing the TFEB-binding region within the *GLA* promoter. We found that incubation with TFEB-WT or TFEB-K116Q, but not TFEB-3KQ or TFEB-K274Q/K279Q, resulted in a strong up-shift of the *GLA* promoter DNA (Fig 5D). These results therefore indicated that acetylation at K274 and K279 reduces the binding of TFEB to its target gene promoters, which was consistent with the ChIP assay results. However, it is noteworthy that TFEB-3KQ or TFEB-K274Q/K279Q incubation, like TFEB-WT or TFEB-K116Q incubation, reduced the

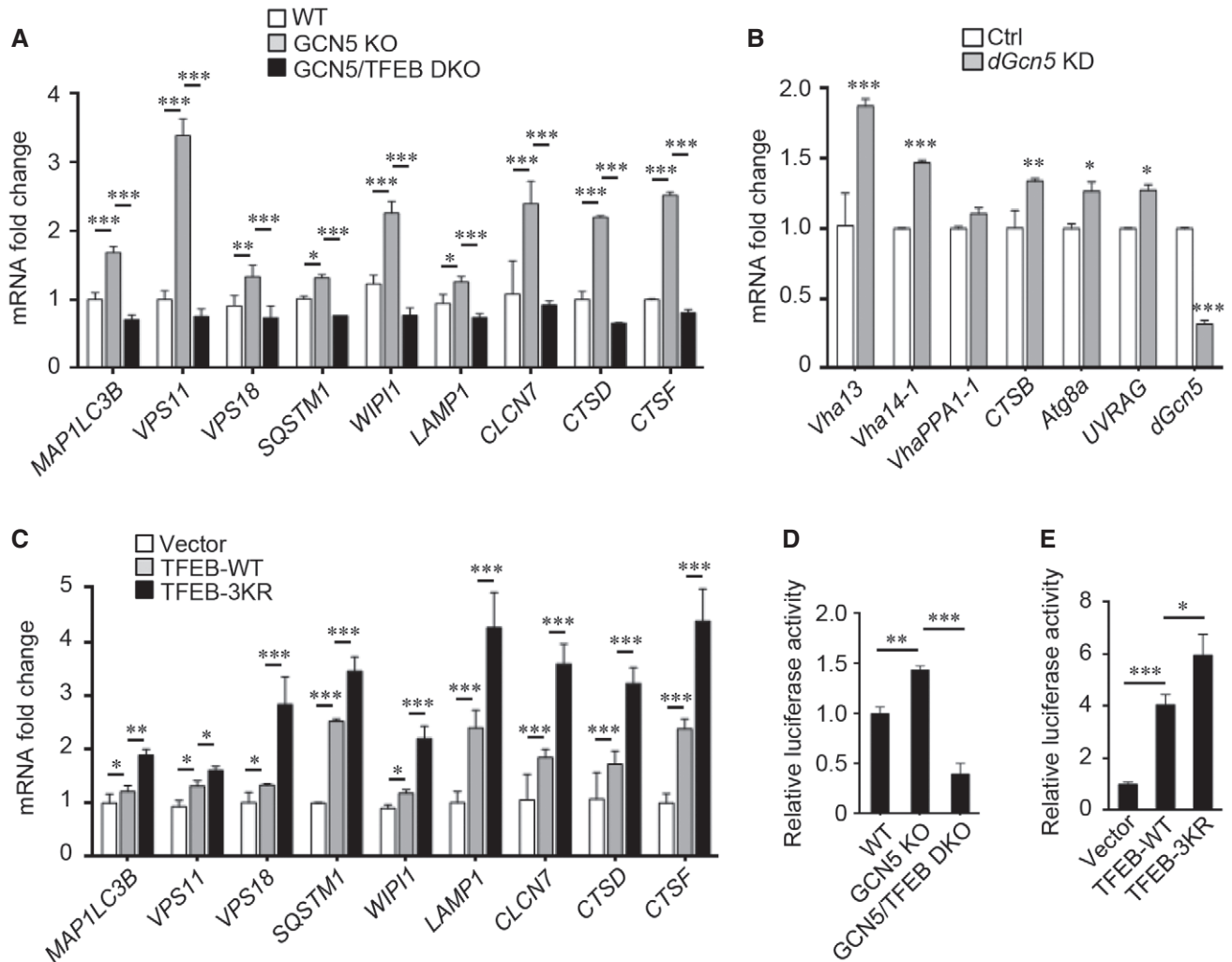


**Figure 4. Acetylation by GCN5 suppresses TFEB transcriptional activity.**

**A** RT-qPCR analysis of the expression of TFEB target genes in WT, GCN5 KO, and GCN5/TFEB DKO HEK293 cells.

**B** RT-qPCR analysis of dMitf target gene expression in *Drosophila* larval fat body with silencing of *dGcn5*.

**C** Expression of TFEB target genes in HEK293 cells transfected with or without TFEB-WT or TFEB-3KR.

**D, E** Luciferase activity measured in WT, GCN5 KO and GCN5/TFEB DKO HEK293 cells (**D**), and in HEK293 cells with TFEB-WT or TFEB-3KR transfection (**E**). The cells were transfected or co-transfected with a TFEB-luciferase reporter. 3KR: Lys 116, Lys 274, and Lys 279 were replaced by Arg.

Data information: In this Figure, data are presented as mean  $\pm$  SEM;  $n = 3$  independent experiments; \* $P < 0.05$ , \*\* $P < 0.01$ , \*\*\* $P < 0.001$ , Student's *t*-test.

level of free *GLA* promoter DNA (Fig 5D). Meanwhile, incubation with TFEB-3KQ or TFEB-K274Q/K279Q caused a smeared up-shift of the *GLA* promoter DNA (Fig 5D). These observations implied that acetylation at K274/K279 may influence the stability of TFEB-DNA binding instead of the constitutive capacity of TFEB for DNA association.

It has been reported that high-affinity DNA binding of TFEB requires TFEB to form homodimers or heterodimers with other members of the MiT/TFE family [39]. Both K274 and K279 are located in helix 2 of the bHLH domain, which is conserved in all the MiT/TFE family proteins and necessary for the formation of homodimers or heterodimers [40,41]. Structural modeling predicts that the substitution of K-to-Q but not K-to-R at K274 and K279 may cause steric hindrance between TFEB and its dimeric partner (Fig 5E).

This suggests that acetylation of these residues may affect TFEB dimerization. To test this, we performed co-immunoprecipitation analysis in cells co-transfected with Myc-labeled and Flag-labeled TFEB or the acetylation-mimetic TFEB mutants. Interestingly, co-precipitations occurred between TFEB-WT, TFEB-WT, and TFEB-K116Q, but not between TFEB-WT and TFEB-K274Q/K279Q (Figs 5F and EV4H). TFEB-K274Q/K279Q also showed weaker interaction with MITF and TFE3 (Figs 5G and H, and EV4I and J). Further, we performed *in vitro* glutaraldehyde cross-linking analysis of purified recombinant TFEBs. In the presence of glutaraldehyde, TFEB-K274Q/K279Q formed fewer dimers than TFEB-WT and TFEB-K116Q (Figs 5I and EV4K). Taken together, these results suggest that acetylation at K274/K279 by GCN5 hinders the binding of TFEB to DNA by interfering with TFEB dimerization.

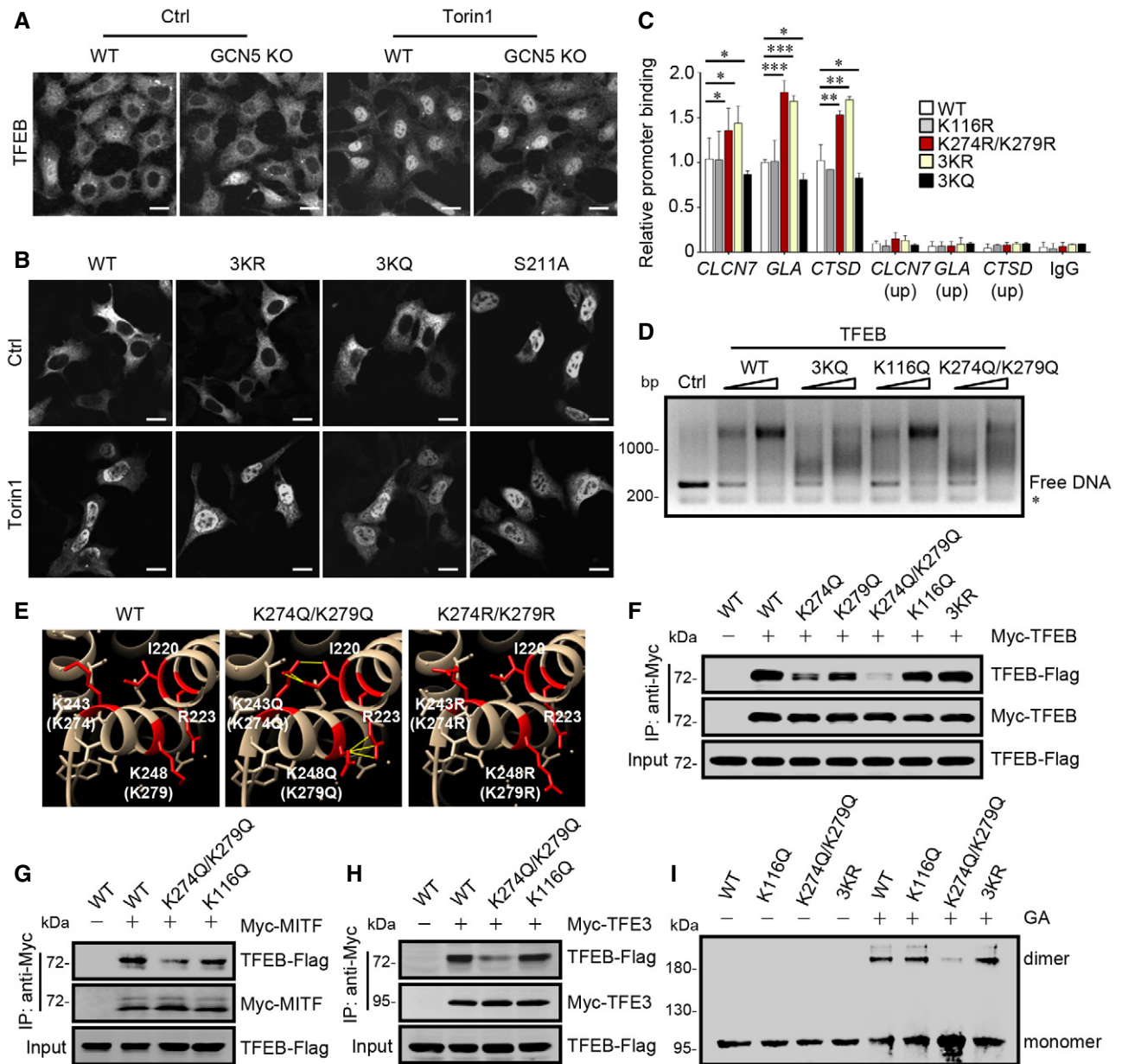


**Figure 5. Acetylation at K274 and K279 disrupts the dimerization and DNA binding of TFEB.**

- A** Subcellular localization of TFEB in WT or GCN5 KO HEK293 cells treated with or without Torin1 (Scale bars, 10  $\mu$ m).
- B** Subcellular localization of Flag-tagged TFEB or TFEB mutants in HEK293 cells treated with or without Torin1. Cells were stained with anti-Flag antibody (Scale bars, 10  $\mu$ m).
- C** ChIP-qPCR analysis of TFEB binding to the promoter of its target genes *CLCN7*, *GLA*, and *CTSD*. Normal mouse IgG and primers against the upstream region lacking CLEAR sites (up) were used as negative controls (mean  $\pm$  SEM;  $n = 3$  independent experiments; \* $P < 0.05$ , \*\* $P < 0.01$ , \*\*\* $P < 0.001$ , Student's  $t$ -test).
- D** Electrophoresis mobility shift assay of TFEB binding to the promoter of *GLA*. A DNA fragment from the *GLA* promoter containing the TFEB-binding site was incubated with purified recombinant TFEB or each of the TFEB mutants, and was subjected to electrophoresis. Asterisk indicates the DNA fragment from the *GAPDH* promoter which was used as a TFEB non-binding DNA control.
- E** Molecular dynamics snapshot of homodimer formation by human MITF and MITF mutants. K243 and K248 in the bHLH-Zip domain of human MITF correspond to K274 and K279 in human TFEB, respectively. Steric interference is shown by yellow lines. Images were created using Chimera (<http://www.cgl.ucsf.edu/chimera/>) and Protein Data Bank (PDB) accession 4ATH.
- F** Co-precipitation of Flag-tagged TFEB and TFEB mutants with Myc-TFEB in HEK293T cells. Immunoprecipitation was carried out with anti-Myc beads, and the precipitates were analyzed using anti-Flag.
- G, H** Co-precipitation of Flag-tagged TFEB and TFEB mutants with Myc-tagged MITF (G) or TFE3 (H) in HEK293T cells.
- I** TFEB homodimer formation detected by glutaraldehyde (GA) cross-linking. Purified recombinant GST-tagged TFEB or TFEB mutants were incubated with or without glutaraldehyde; then, the products were analyzed by immunoblotting using anti-TFEB.

Source data are available online for this figure.



So far, phosphorylation-dependent translocation from the cytoplasm to the nucleus is the main regulatory pathway for TFEB activation [4–6,42]. In order to provide more direct evidence that GCN5 modifies TFEB in the nucleus, thereby affecting its DNA binding, we examined the effect of GCN5 on the dimerization of a TFEB mutant, in which both of the known phosphorylation sites S142 and S211

were substituted by alanine (TFEB-2SA) and were specifically localized in the nucleus (Fig EV4L). We observed a strong co-precipitation between TFEB-2SA-Flag and TFEB-2SA-Myc, which was decreased by overexpression of GCN5 and increased by GCN5 knockdown (Fig EV4M). Accordingly, induction of TFEB-2SA-Flag enhanced the activity of the TFEB-luciferase reporter, and the

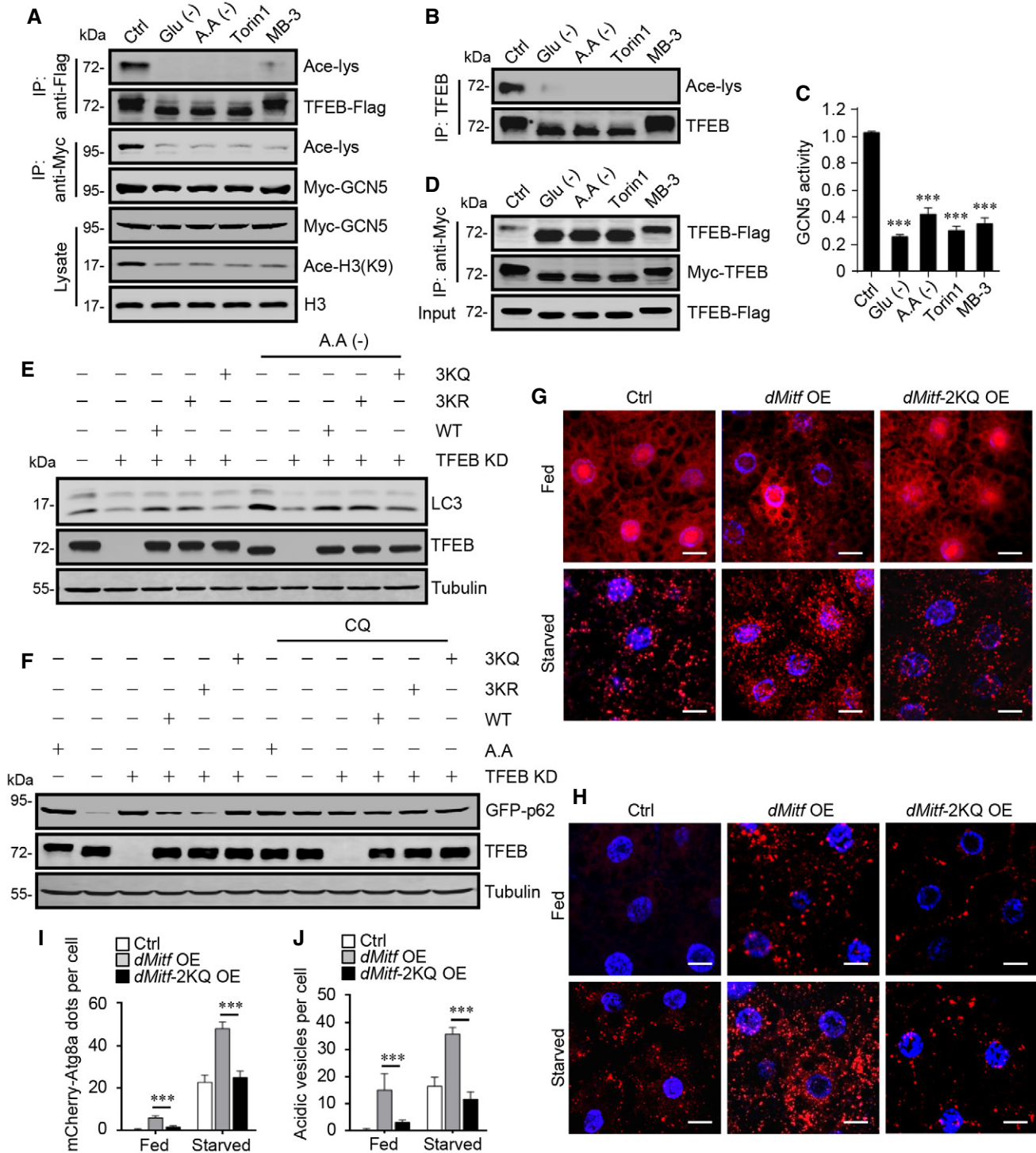


Figure 6.

**Figure 6. GCN5-mediated TFEB acetylation in autophagy.**

- A Acetylation of TFEB-Flag, Myc-GCN5, and histone H3 in HEK293 cells. The cells were either starved of glucose or amino acids or treated with Torin1 or MB-3.
- B Acetylation of endogenous TFEB in HeLa cells. The cells were treated as in (A).
- C GCN5 activity measured by *in vitro* acetylation assay using Myc-GCN5 immunoprecipitated from HEK293T cells and purified histone H3 as the substrate. (mean  $\pm$  SEM;  $n = 3$  independent experiments; \*\*\* $P < 0.001$ , Student's *t*-test).
- D Co-precipitation of TFEB-Flag with Myc-TFEB in HEK293 cells treated as in (A).
- E LC3-II formation in HeLa cells transfected with Flag-tagged TFEB or TFEB mutants after TFEB RNAi. The cells were treated with or without amino acid starvation.
- F GFP-p62 levels in HEK293 cells stably expressing GFP-p62. The cells were treated as in (E), with or without addition of CQ.
- G, H Representative images of mCherry-Atg8a (red) (G) and LysoTracker (red) staining (H) in *Drosophila* larval fat body in which dMitf or dMitf-2KQ (K445Q/K450Q) was overexpressed. *Drosophila* (cg-GAL4/+) was used as the control, and DAPI staining (blue) was used to indicate the cell nucleus (Scale bars, 10  $\mu$ m).
- I, J Quantification of mCherry-ATG8a puncta (I) and LysoTracker puncta (J) in (G) and (H), respectively (graph represents data from three independent experiments with  $\geq 30$  cells per condition; mean  $\pm$  SEM; \*\*\* $P < 0.001$ , Student's *t*-test).

Source data are available online for this figure.

enhancement was attenuated by GCN5 overexpression and promoted by GCN5 knockdown (Fig EV4N).

### Acetylation of TFEB suppresses autophagy and lysosome biogenesis

We then assessed the biological significance of GCN5-mediated TFEB acetylation by examining its role in autophagy. First, in glucose- or amino acid-starved cells and cells treated with Torin1 and MB-3, we observed significant decreases in acetylation of GCN5 and TFEB (Fig 6A and B), which were accompanied by decreased GCN5 activity (Fig 6C) and increased dimerization of TFEB (Fig 6D). These observations suggested that GCN5 was inactivated and TFEB was activated upon autophagy induction. Next, we found that in both normal culture and amino acid starvation conditions, overexpression of TFEB-WT or TFEB-3KR restored the decreased intracellular LC3 level caused by TFEB knockdown, while TFEB-3KQ was less effective (Figs 6E and EV5A). In addition, when TFEB knockdown inhibited the decrease in intracellular GFP-p62 triggered by amino acid deprivation in cells stably expressing GFP-p62, transfection of TFEB-WT or TFEB-3KR prevented the inhibition, while TFEB-3KQ was less effective (Figs 6F and EV5B). Further, we analyzed the effect of dMitf acetylation on autophagosome and lysosome biogenesis in *Drosophila*. Consistent with previous reports [43,44], overexpression of dMitf increased the mCherry-Atg8a puncta and LysoTracker-labeled puncta in the fat body of fed *Drosophila* larvae and further promoted the formation of puncta in starved *Drosophila* larvae (Fig 6G–J). In comparison, overexpression of the dMitf-K445Q/K450Q (2KQ) mutant hardly influenced the number of mCherry-Atg8a puncta and starvation-induced LysoTracker puncta (Fig 6G–J). Together, these data suggest that GCN5-mediated TFEB acetylation inhibits autophagy and lysosomal biogenesis. The low but detectable formation of LysoTracker puncta in fed dMitf-2KQ-overexpressing *Drosophila* (Fig 6H and J) suggests that lysosome biogenesis may be more sensitive to TFEB activity than autophagosome formation.

### Silencing dGcn5 facilitates the clearance of Tau aggregates in *Drosophila*

Finally, we applied a *Drosophila* neurodegeneration model to further evaluate the physiological function of the GCN5-TFEB pathway. Using the retina-specific glass multiple repeat enhancer (GMR)-Gal4 driver, we ectopically expressed the human microtubule-associated

protein hTau in *Drosophila* eyes. This led to the formation of hTau aggregates and neurotoxicity which presented as a rough ocular phenotype [45,46] (Fig 7A, C and D). The introduction of exogenous dMitf improved the degenerative phenotype and reduced hTau aggregation, which were missing in CQ-fed *Drosophila* (Fig 7A, C and D), supporting previous observations in mouse brain models [47]. Surprisingly, the introduction of dMitf-2KQ aggravated rather than improved the aggregation and neurotoxicity of hTau (Fig 7A, C and D). The phenotype was very similar to that of dMitf KD *Drosophila* (Fig 7A, C and D), suggesting dMitf-2KQ may play the role of dominant negative mutant. In addition, knocking down dGcn5 in the *Drosophila* eyes reduced hTau aggregation and mitigated the neurotoxic phenotype (Fig 7B–D). In *Drosophila* with dAtg7 KD or fed with CQ, the effect of dGcn5 silencing disappeared (Fig 7B–D), which suggests that it is dependent on the activation of autophagy.

## Discussion

To date, the study of GCN5 in cell metabolism has mainly focused on its regulation of PGC-1 $\alpha$ , the transcriptional coactivator for the expression of genes involved in mitochondrial functional. Here, our results demonstrate that GCN5 is a direct modulator of TFEB, the master transcription factor for cell autophagy and lysosomal biogenesis. This mechanism suggests that GCN5 not only regulates the recycling of nutrients and energy in cells, but also plays a role in the digestion and clearance of intracellular protein aggregates and impaired organelles, which are crucial for cell metabolism and growth.

By demonstrating that GCN5 modifies TFEB through acetylation at specific sites, we have uncovered novel molecular mechanisms for the regulation of this important transcription factor. Our discovery will also contribute to the dissection of lysosome-related intracellular functions, especially the coupling of cell metabolism status with lysosome biogenesis. While the regulation of TFEB through its phosphorylation status has been widely recognized, our results clearly show that GCN5-mediated acetylation inhibits TFEB transcriptional activity without affecting its subcellular localizations. The evidence provided by this study strongly suggests that the acetylation by GCN5 serves as an additional step for controlling the activity of TFEB after it enters the nucleus. Despite the lack of direct evidence, it has recently been proposed that TFEB dimerization occurs in the cytoplasm and is necessary for nuclear translocation of TFEB [48]. With co-immunoprecipitation analysis, it has been

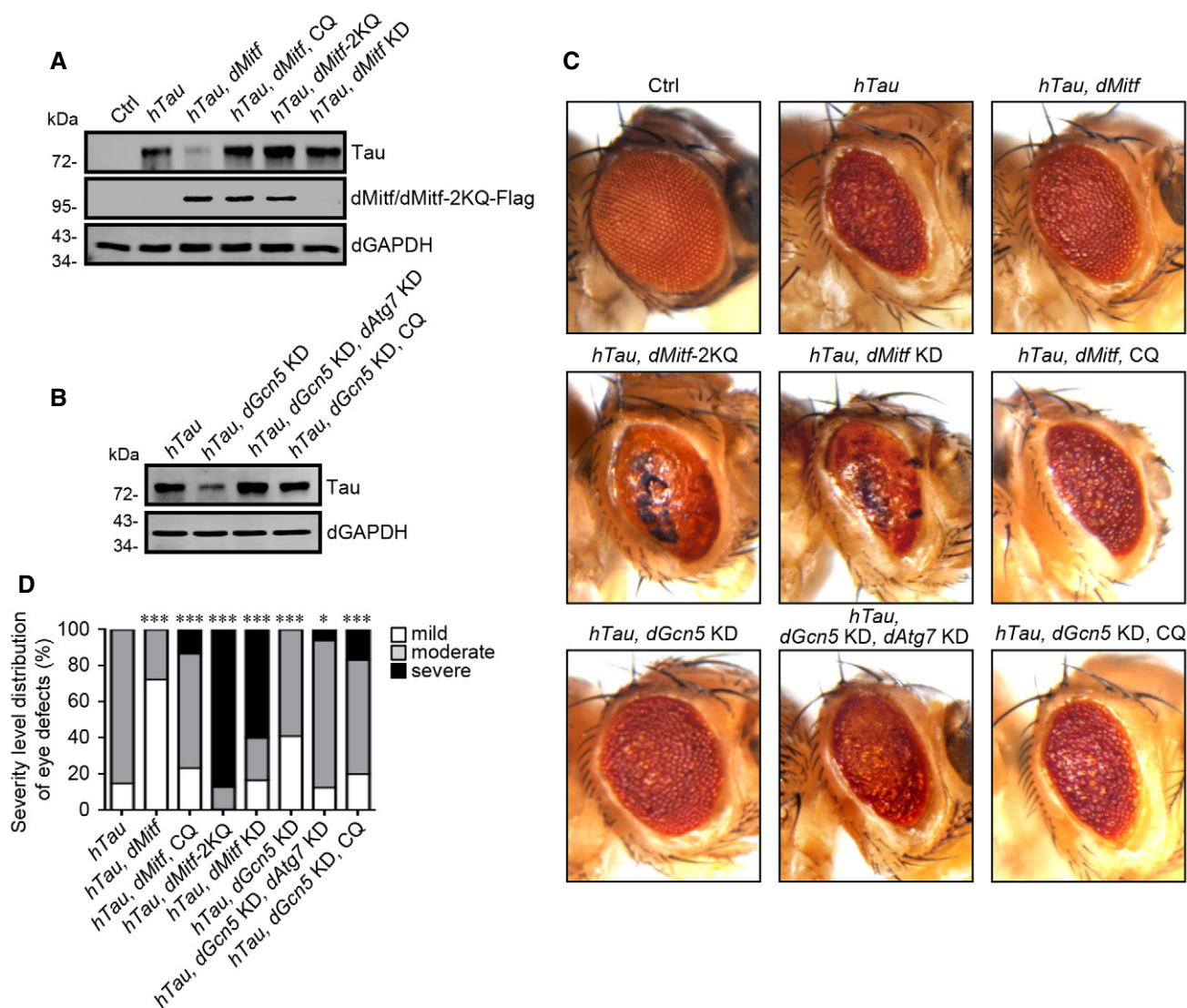


**Figure 7. Silencing dGcn5 facilitates the clearance of Tau aggregates.**

A, B The level of insoluble Tau protein in the head of adult *Drosophila* with or without CQ feeding. The indicated genes were transgenically expressed in the eyes of the *Drosophila* using the GMR-Gal4 driver. *Drosophila* (GMR-Gal4/+) was used as the control.

C Representative light micrographs of adult *Drosophila* eyes expressing the indicated transgenes under the control of the GMR-Gal4 driver. The *Drosophila* were fed with or without CQ. *Drosophila* (GMR-Gal4/+) was used as the control.

D Distribution of the different eye phenotypes following genetic manipulations in (C). The *Drosophila* were fed with or without CQ (30 flies per condition were randomly selected for analyses; \* $P < 0.05$ , \*\*\* $P < 0.001$ , chi-square test).

Source data are available online for this figure.

shown that the phosphorylation-disabled TFEB-S142A/S211A can form dimers with the phosphorylation-mimic TFEB-142D/211D, and the ratio of phosphorylated-non-phosphorylated TFEB heterodimer to non-phosphorylated TFEB homodimer may affect the efficiency of TFEB nuclear entry [48]. However, it seems that the TFEB dimer may be formed in the nucleus. Theoretically, the different localizations of phosphorylated TFEB and non-phosphorylated TFEB may prevent them from forming dimers. In addition, we show that acetylation of nuclear TFEB can significantly inhibit its dimerization. While the possibility that acetylation may disrupt dimeric TFEB cannot be ruled out, another possibility is that replacing S142 and

S211 with aspartic acid may not mimic the phosphorylation of TFEB in the detection of dimer formation, because we observed an obvious distribution of TFEB-S142D/S211D in the cell nucleus (Appendix Fig S1).

K116 has previously been reported as an acetylation-competent residue on TFEB [11,16]; however, the effect of acetylation at this site on TFEB activity was unclear. While deacetylation of K116 by Sirt1 was linked to enhanced lysosomal biogenesis [11], its acetylation in cells treated with deacetylase inhibitors was involved in the activation of lysosomal and autophagy processes [16]. We found that K116 is a target site of GCN5, and its acetylation leads to a

decrease in the expression of TFEB target genes (Appendix Fig S2). However, compared with K274 and K279, which are more conserved between species, acetylation of K116 has little effect on the dimerization and DNA binding of TFEB. Structurally, K116 is located near the transactivation domain of TFEB, which contributes to TFEB transcriptional activity mainly by recruiting transcriptional coactivators and facilitating the assembly of transcription initiation complexes [49,50]. We propose that acetylation at K116 influences the interaction of TFEB with its coactivators, and because K116 is not conserved in other members of the MiT/TFE family, K274 and K279 may play a leading role in regulating TFEB activity. In addition, based on our results from *Drosophila* showing that overexpression of *dMitf*-2KQ leads to aggravated aggregation and neurotoxicity of hTau, we propose that acetylation at K274 and K279 may play the role of dominant negative mutation. It is possible that acetylated TFEB competes with deacetylated TFEB for the binding of CARM1 (unpublished data), which is a coactivator of TFEB that regulates the transcription activity of TFEB [51].

It has been shown that mTORC1 exhibits kinase activity in the cell nucleus and acetyltransferase p300 can be directly phosphorylated and activated by mTORC1 [52–54]. In this study, we showed that GCN5 is significantly inactivated in amino acid-starved cells and Torin1-treated cells, which strongly suggests a potential regulatory role of mTORC1 on GCN5. This regulation may coordinate with the mTORC1-controlled nuclear entry–exit events of TFEB [55], enabling the cell to maintain low TFEB transcriptional activity under growth conditions. Upon cell stress, the inactivation of mTORC1 leads not only to accumulation of TFEB in the nucleus, but also to binding of TFEB to the promoters of its target genes through inactivation of GCN5, thus increasing the lysosome biogenesis and autophagy flux. Although the regulatory effect of mTORC1 on GCN5 remains to be confirmed by future studies, our results demonstrate that the GCN5-TFEB pathway plays an important role in clearing protein aggregates in cells, and may be a potential therapeutic target for neurodegenerative diseases.

## Materials and Methods

### Cell culture and treatment

HEK293, HEK293T, MEF, and HeLa cells were grown in Dulbecco's modified Eagle Medium (DMEM; Gibco) supplemented with 10% FBS in a 37°C incubator with a humidified, 5% CO<sub>2</sub> atmosphere. *Drosophila* S2 cells were cultured in Schneider's *Drosophila* medium (Sigma-Aldrich) supplemented with 10% heat-inactivated FCS in a 25°C incubator.

Unless otherwise stated, the chemicals were used as follows: Torin1, 250 nM, 4 h; MB-3, 50 μM, 16 h; chloroquine, 50 μM, 4 h; bafilomycin A1 (Baf), 100 nM, 4 h; and C646 10 mM, 4 h.

### Antibodies

Antibody to dGAPDH is kindly provided by Dr. Wanzhong Ge. Antibodies to Ace-lys (9441), TFEB (4240), Ace-H3 (K9) (9649), Ace-H3 (K27) (4353), histone H3 (4499), 4E-BP1 (9644), and P-4E-BP1 (Thr37/46) (2855) were purchased from Cell Signaling Technology; antibodies to IFT20 (13615), PDLIM1 (11674), β-Actin (66009), and

p62 (18420) were purchased from Proteintech; antibodies to GFP (M048-3), α-Tubulin (M175-3), Myc (M192-3S), Flag (M185-3B), HA (M180-3S), and GST (M071) were purchased from MBL; antibodies to LC3 (L7543) and Tau (T9450) were purchased from Sigma; antibodies to CTSD (136282), LAMP1 (17768), and GCN5 (365321) were purchased from Santa Cruz; antibody to EGFR (db1025) was purchased from Diabio.

### *Drosophila* stocks

All *Drosophila* stocks were reared on a standard cornmeal medium in 25°C incubators under a 12-h:12-h light:dark cycle [56]. CQ (Sigma-Aldrich) as a 100-mM stock solution was freshly prepared in H<sub>2</sub>O and dissolved into *Drosophila* media at 10 mM. The GMR-Gal4 *Drosophila* strain was kindly provided by Dr. Wanzhong Ge. The *cg-Gal4* and *mCherry-Atg8a* *Drosophila* strains were kindly provided by Dr. Chao Tong. *dGcn5* KD (line BL9332) and *hTau* (line BL51363) were purchased from the Bloomington Stock Center (Bloomington, IN). *dMitf* KD (line THU3522) and *dATG7* KD (line THU1583) were purchased from the Tsinghua Fly Center (THFC). All genotypes of fly strains generated in the paper were added as Appendix Table S1. RNAi efficiency in *Drosophila* is presented in Appendix Fig S3.

### Site-directed mutagenesis and *Drosophila* transformation

To generate transgenic *Drosophila*, cDNA encoding full length *dGcn5* and *dMitf* were cloned into pUAST-attB vector. cDNA was reversely transcribed using M-MLV reverse transcription reagents (Promega) with RNA extracted from *Drosophila* head. pUAST-attB vector containing *dMitf*-Flag was used as the template to generate various *dMitf* mutants via site-directed mutagenesis. pUAST-attB vector containing Flag-tagged *dMitf*, *dMitf*-2KQ, and *dGcn5* were sequence confirmed and germline transformed into *Drosophila* (Core Facility of *Drosophila* Resource and Technology, SIBCB, CAS). All of the genetic manipulations in our study were based on *Drosophila* *w*<sup>1118</sup>.

### Transfection

Transient transfection of DNA in mammalian cells was performed using Lipofectamine 2000 (Invitrogen) according to the manufacturer's instructions. Cells were analyzed 18–24 h after transfection. Transient transfection of DNA in *Drosophila* S2 cells was performed using Lipofectamine 3000 (Invitrogen) according to the manufacturer's instructions. S2 cells were analyzed 48 h after transfection.

For RNA interference in mammalian cells, siRNA duplexes designed against conserved targeting sequences were transfected using Lipofectamine 2000 for 72 h. The following siRNA duplexes were used: GCN5 siRNA: CCGGAAGCUCACUGGCAUG; TFEB siRNA: AAACGGAGCCUACUGAACA. RNA interference in *Drosophila* cells was described in [Ref. 57]. First, dsRNA targeting *dGcn5* is generated by a two-step PCR and *in vitro* transcription. In the first step, T7 RNA polymerase promoter sequence was fused to the sequences of *dGcn5*. These are linked to T7 sequences to enable an *in vitro* transcription with T7-RNA polymerase. 1 μg PCR product was used as a template. 100 μg double-stranded RNAs (dsRNAs) were generated in a 50 μl transcription reaction using the RiboMAX

Large Scale RNA Production Systems (Promega). The primers used were as follows: *dGcn5* F: 5'-CTCACTATAGGGAGAAGCGAATGGCG CAGCAACCG-3'; *dGcn5* R: 5'-CTCACTATAGGGAGACCTGGTCGA CGGCGATTCAA-3'; T7 promoter primer: GAATTAATACGACTCAC TATAGGGAGA. S2 cells were resuspended in serum-free medium and incubated with the dsRNAs at room temperature for 30 min. Cells were analyzed 72 h after transfection.

### RNA extraction and quantitative PCR

Total RNA was extracted from cells or *Drosophila* tissues using TRIzol (Invitrogen). cDNA was reversely transcribed using M-MLV reverse transcription reagents (Promega). Quantitative PCR was performed with SYBR Premix Ex Taq (TaKaRa) on a 7300 Real-Time PCR System (Applied Biosystems). Gene expression levels were calculated according to the  $2^{-DDCt}$  method and normalized against  $\beta$ -Actin or Act5C (*Drosophila*). Primers used for RT-PCR were listed in Appendix Table S2 (human cells) and Appendix Table S3 (*Drosophila*).

### Immunostaining

Cells were cultured on coverslips and fixed in 4% formaldehyde for 10 min at room temperature. After washed three times with PBS, cells were incubated in PBS containing 10% FBS to block non-specific sites of antibody adsorption. Then, the cells were incubated with primary and secondary antibodies in PBS containing 0.1% saponin and 10% FBS. *Drosophila* fat bodies were dissected in cold PBS from the third-instar larvae and then fixed in 4% formaldehyde for 20 min. After washed three times with PBST (PBS + 0.1% Triton X-100), tissues were incubated with DAPI at room temperature for 1 h. After extensive wash, samples were mounted in vector shield.

Confocal images were captured in multitracking mode on an LSM800 Meta laser-scanning confocal microscope (Carl Zeiss) with a 63 $\times$  Plan Aplanachromat 1.4 NA objective and analyzed with the ZEN 2012 software.

### Light microscopy and qualitative analysis of eye phenotypes

The *Drosophila* eye images were captured using a Nikon SMZ18 microscope. Ten images with sequential focal points were taken to cover an entire eye, and these images were reconstituted to a fully focused final image using the NIS-Elements (version 3.0).

To apply quantitative analysis, we randomly selected 30 3-day-old female flies per genotype and classified phenotypic severity using objective features. The eye defects observed were classified into three classes according to their severity, as previously described [58]: Category 1 had mucosal eyes but with normal morphology (mild); category 2 exhibited disorganized ommatidial array (moderate); and category 3 had black spots of necrotic tissue on their eyes (severe).

### Stable cell line construction

pEP-GCN5-KO plasmid was made by cloning the target DNA sequence of human GCN5 (GGGGGATCCGGCTCGACC) into a pEP-KO Z1779 vector using SapI. GCN5 KO HEK293/HeLa cells were created by transient transfection of pEP-GCN5-KO plasmid

followed by selection with 2.5  $\mu$ g/ml puromycin. pEP-TFEB-KO plasmid was made by cloning the target DNA sequence of human TFEB (AGTACCTGTCCGAGACCTAT) into a pEP-KO Z1779 vector using Sap I. GCN5/TFEB DKO HEK293/HeLa cells were created by transient transfection of pEP-TFEB-KO plasmid into GCN5 KO HEK293/HeLa cells followed by selection with 2.5  $\mu$ g/ml puromycin.

HEK293 cells stably expressing GFP-p62 were created by transient transfection followed by selection with G418 (500  $\mu$ g/ml) for 2 weeks.

### Immunoblotting and immunoprecipitation

Mammalian cells were harvested and lysed in Nonidet P-40 (NP-40) lysis buffer (20 mM Tris-HCl, pH 7.5, 0.5% NP-40, 1 mM MgCl<sub>2</sub>, 137 mM NaCl, 1 mM CaCl<sub>2</sub>, 10% glycerol, 1 mM Na<sub>4</sub>P<sub>2</sub>O<sub>7</sub>, 1 mM Na<sub>3</sub>VO<sub>4</sub>, 10 mM NaF, 1 mM TSA, 5 mM NAM). *Drosophila* cells were harvested and lysed in lysis buffer (25 mM Tris-HCl, pH 8.0, 27.5 mM NaCl, 20 mM KCl, 25 mM sucrose, 10 mM EDTA, 10 mM EGTA, 0.5% NP-40, 10% glycerol, 1 mM DTT). All buffers used throughout processing contained protease inhibitors. Proteins were denatured and resolved on sodium dodecyl sulfate-polyacrylamide gels (SDS-PAGE) and then transferred to a polyvinylidene difluoride membrane. After blocking with 5% (w/v) bovine serum albumin, the membrane was stained with the corresponding primary antibodies and secondary antibodies. Specific bands were analyzed using an Odyssey infrared imaging system (LI-COR Biosciences). Protein bands were quantified using the ImageJ software.

For immunoprecipitation, cell lysates were mixed with antibodies at 4°C overnight, followed by the addition of protein A/G agarose beads for 2 h. Then, immunocomplexes were washed five times using lysis buffer and subjected to immunoblotting.

Nonionic detergent soluble and insoluble hTau fractions were prepared using a previously described method [59]. Briefly, *Drosophila* heads were homogenized in TNE buffer (10 mM Tris-HCl, pH 7.4; 150 mM NaCl; 5 mM EDTA) containing protease inhibitor cocktail and 0.5% NP-40. After centrifugation at 10,000 g for 10 min at 4°C, supernatant was collected as soluble fraction. The pellet was washed once in TNE buffer and solubilized in TNE buffer containing 1% SDS. Protein concentrations in the supernatants were measured with a BCA protein assay kit. Equivalent amounts of soluble and insoluble proteins from different flies were separated by SDS-PAGE for immunoblotting.

### Glutaraldehyde cross-linking

In a 20  $\mu$ l reaction system, 100  $\mu$ g purified proteins of GST-tagged TFEB or TFEB mutants were incubated with 0.003% of glutaraldehyde within reaction buffer (10 mM Tris pH 8.0, 140 mM NaCl, 0.5% NP-40) at 25°C for 5 min. The reaction was stopped by adding protein sample buffer, and the samples were analyzed by immunoblotting.

### Subcellular fractionation

Cell pellets were washed with PBS and resuspended in lysis buffer (10 mM HEPES, pH 7.4, 10 mM KCl, 1.5 mM MgCl<sub>2</sub>, 0.5 mM DTT). The suspension was put on ice for 30 min. After centrifugation at

500 g for 5 min at 4°C, the supernatant was collected as cytosolic fraction. The pellet was washed twice with lysis buffer and resuspended in 0.5% NP-40 lysis buffer. After centrifugation at 15,000 g for 15 min, the resultant supernatant was used as the nuclear fraction. All buffers used throughout processing contained protease inhibitors.

### β-Hexosaminidase assay

Lysosomal β-hexosaminidase assay was described in [Ref. 60]. Equal numbers ( $1 \times 10^6$  cells) of HEK293 cells (WT or GCN5 KO) were lysed in 150 μl 0.1% Triton X-100 containing protease inhibitor cocktail for 20 min and centrifuged at 10,000 g. 20 μl of 1 mM p-nitrophenyl-N-acetyl-β-D-glucosaminide (p-NAG) (Sigma-Aldrich, Cat#: N9376) was incubated with 20 μl of each clarified sample at 37°C for 1 h. 250 μl of 0.1 M Na<sub>2</sub>CO<sub>3</sub>/NaHCO<sub>3</sub> solution was added to stop the reaction. The reaction product was measured by reading the absorbance at 405 nm immediately.

### LysoTracker staining

Cells were cultured on coverslips and incubated for 30 min with 50 nM LysoTracker red (DND-99; Life Technologies, L-7528). Cells then were washed twice with PBS and visualized in PBS containing DAPI.

*Drosophila* fat bodies were dissected in cold PBS from the third-instar larvae and incubated in PBS containing 1 μM LysoTracker red at room temperature for 45 min. After washed three times with PBS, tissues were transferred to Schneider's *Drosophila* medium (Sigma-Aldrich) with DAPI on glass slides, covered, and immediately photographed live on LSM800 Meta laser-scanning confocal microscope. Acidic vesicles were counted manually using ImageJ software analysis.

### FACS analysis

Cells were cultured in 50 nM LysoTracker red for 30 min. Then, cells were trypsinized and washed with PBS. Red lysosomal fluorescence of 10,000 cells per sample was determined by flow cytometry using the Cytomic FC 500MCL (BECKMAN COULTER).

### Recombinant protein purification and *in vitro* acetylation assay

GST-TFEB was expressed in *Escherichia coli* BL21. Bacteria were treated with 0.1 mM IPTG at 30°C to induce protein expression, and were harvested and resuspended in lysis buffer (PBS containing 0.5% Triton X-100, 2 mM EDTA, and 1 mM PMSF), followed by ultrasonication. The recombinant TFEB proteins were purified using glutathione-sepharose 4B beads. Then, the beads were centrifuged by gentle rotation at 4°C and washed three times with 10 ml lysis buffer, then suspended with TEV cleavage buffer (10 mM Tris-HCl, pH 8.0, 150 mM NaCl, 0.1% NP-40, 1 mM DTT, 1 mM EDTA). 80 μl TEV protease (kindly provided by Sun' lab) was added, and incubation was performed overnight by gentle rotation at 4°C. The supernatant (containing recombinant TFEB proteins) was obtained by centrifuging.

Myc-GCN5 protein was purified from HEK293T cells 24 h after transfection by immunoprecipitation with anti-Myc affinity beads

(Selleck). For *in vitro* acetylation assay, TFEB protein (10 mg) was incubated with Myc-GCN5 immunoprecipitated from cell lysate, in the presence of acetyl-coenzyme A (4 mg) and 10 μl 5× HAT assay buffer (250 mM Tris-HCl, pH 8.0, 5 mM dithiothreitol, 50% glycerol, 0.5 mM EDTA) in a total volume of 50 μl. The contents were gently mixed and placed in a 30°C shaking incubator for 1 h. Then, protein loading buffer was added to the reaction and boiled for 5 min. The reaction products were separated by SDS-PAGE for immunoblotting or Coomassie Blue staining. Specific band was cut off and subjected to HPLC-MS/MS.

### Fluorometric GCN5 activity assay

Myc-GCN5 was immunoprecipitated from HEK293T cells. The immunoprecipitated proteins were incubated with acetyl-CoA and peptide substrate histone H3 at 37°C for 15 min according to the manufacturer's protocol (Active Motif #56100). The reaction was stopped with Stop Solution, followed by further incubation with Developer Solution for 15 min in the dark at room temperature. The activity of GCN5 was assessed by measuring the fluorescent emission at 460 nm following excitation at 380 nm.

### HPLC-MS/MS

To identify the acetylation site of TFEB by mass spectrometry, the gel band of acetylated TFEB was cut off. In-gel digestion of TFEB was performed with MS-grade modified trypsin (Promega) at 37°C overnight. The digested peptides were loaded on an in-house packed capillary reverse-phase C18 column (15 cm in length, 3 mm particle size, 100 mm ID 3 360 mm OD, 100 Å pore diameter) connected to an Easy LC 1000 system. The samples were analyzed with a 180 min-HPLC gradient from 0% to 100% buffer B (0.1% formic acid in acetonitrile) at 300 nl/min. The eluted peptides were ionized and directly introduced into a Q-Exactive or Fusion mass spectrometer (Thermo) using a nano-spray source. Survey full-scan MS spectra ( $m/z$  300–1,800) were acquired in the Orbitrap analyzer with resolution  $r = 70,000$  at  $m/z$  400.

### Luciferase assays

The TFEB-luciferase construct which contains 4× CLEAR sites before luciferase reporter was provided by Dr. A. Ballabio [3]. HEK293 cells were transfected with indicated Flag-tagged TFEB or mutant plasmids for 24 h using Lipofectamine 2000 (Invitrogen). Then, cells were transfected with TFEB-luciferase construct for another 48 h, and luciferase assays were performed using a Dual-Luciferase Reporter Assay System (Promega) based on the protocol provided by the manufacturer.

### ChIP assay

HeLa cells were transfected with Flag-tagged TFEB or mutants for 48 h. Then, cells were incubated in 1% formaldehyde for 10 min at room temperature to crosslink DNA to associated proteins. A final concentration of 0.125 M glycine was added to stop the cross-linking reaction. Cells were washed twice by cold 1× PBS and lysed with SDS lysis buffer (50 mM Tris-HCl, pH 8.1, 10 mM EDTA, pH 8.0, 1% SDS) containing protease inhibitors. After 30 min of

incubation on ice, lysates were centrifuged for 5 min at 800 g and 4°C, and the nuclear pellets were collected and sonicated in SDS lysis buffer. For immunoprecipitation, 200 µl of chromatin was diluted 1:5 in ChIP dilution buffer (16.7 mM Tris-HCl, pH 8.1, 0.01% SDS, 1.1% Triton X-100, 1.2 mM EDTA, 167 mM NaCl) and 1% of the diluted sample was set aside for input. The diluted sample was precleared with Protein G beads (Biorworld) at 4°C for 1 h. The precleared lysates were incubated overnight with 1 µg of anti-Flag M2 affinity gel (SIGMA). After immunoprecipitation, the beads were washed at room temperature (for 5 min each) with 700 µl of low-salt buffer (0.1% SDS, 1% Triton X-100, 2 mM EDTA, 20 mM Tris-HCl, pH 8.1, 150 mM NaCl), high-salt buffer (0.1% SDS, 1% Triton X-100, 2 mM EDTA, 20 mM Tris-HCl, pH 8.1, 500 mM NaCl), LiCl buffer (0.25 M LiCl, 1% NP-40, 1% deoxycholic acid, 1 mM EDTA, 10 mM Tris, pH 8.1), and TE buffer (10 mM Tris-HCl, 1 mM EDTA at pH 8.0). Elution was performed twice in 250 µl of fresh elution buffer (1% SDS and 0.1 M NaHCO<sub>3</sub>) for 15 min at room temperature. 20 µl of 5 M NaCl was added, and samples were incubated overnight at 65°C to reverse the crosslinks. Input DNA was diluted in freshly made elution buffer to a volume of 500 µl, and crosslink reversal was performed. After crosslink reversal, samples were digested with 20 µg of proteinase K for 2 h at 45°C, and DNA was recovered by standard methods in 20 µl of 10 mM Tris-HCl at pH 8.0. 1 µl of DNA was used for each quantitative PCR. The quantitative PCR data were analyzed as described previously [61]. The primers used for CHIP-qPCR were listed in Appendix Table S4.

### EGFR degradation assay

After cultured in serum-free DMEM for 12 h, HEK293 or GCN5 KO HEK293 cells incubated on ice in serum-free DMEM medium containing 200 ng/ml of EGF for 15 min. Next, the cells were washed with PBS and cultured in serum-free DMEM at 37°C. At determined time points, the cells were lysed and subjected to immunoblot with EGFR antibody.

### Electrophoretic mobility shift assay

Recombinant protein TFEB and TFEB mutants were purified from *Escherichia coli*. *GLA* promoter DNA fragments and non-specific DNA (*GAPDH* promoter region) were amplified using primers listed in ChIP assay column. DNA was purified by QiAquick PCR purification kit and eluted with ultrapure water. 1 µg of DNA fragments was incubated with purified proteins (25–50 µg) in the *in vitro* binding buffer (10 mM Tris-HCl, pH 7.5, 50 mM KCl, 5 mM MgCl<sub>2</sub>, 1 mM DTT, 2.5% glycerol, 0.05% NP-40, 5 µg/ml salmon sperm DNA) at room temperature for 1 h. Samples were separated by the 1.5% agarose gel and stained with ethidium bromide. The shift of the bound DNAs was visualized under ultraviolet (UV) light.

**Expanded View** for this article is available online.

### Acknowledgements

We thank Dr. Qunying Lei, Dr. Chao Tong, Dr. Wanzhong Ge, Dr. Shengcai Lin, and Dr. Han-Ming Shen for sharing plasmids. We thank Qiang Zhao and Dr. Chen Li for their assistance in structural modeling. We thank Dr. Tianhua Zhou and Dr. Wei Wan for their critical discussion and comments on the manuscript. We are grateful to the Imaging Center of Zhejiang University School of

Medicine for their assistance in confocal microscopy. This study was supported by the National Basic Research Program of China (2017YFA0503402) and the National Natural Science Foundation of China (31790402, 31530040, and 31671434).

### Author contributions

WL, YW, and ZG designed the experiments. YW, YH, JL, ZY, JZ, and MX performed the experiments. CP performed the mass spectrometry. WL and YW wrote the manuscript.

### Conflict of interest

The authors declare that they have no conflict of interest.

## References

- Galluzzi L, Yamazaki T, Kroemer G (2018) Linking cellular stress responses to systemic homeostasis. *Nat Rev Mol Cell Biol* 19: 731–745
- Mizushima N, Levine B, Cuervo AM, Klionsky DJ (2008) Autophagy fights disease through cellular self-digestion. *Nature* 451: 1069–1075
- Sardiello M, Palmieri M, di Ronza A, Medina DL, Valenza M, Gennarino VA, Di Malta C, Donaudo F, Embrione V, Polishchuk RS *et al* (2009) A gene network regulating lysosomal biogenesis and function. *Science* 325: 473–477
- Settembre C, Di Malta C, Polito VA, Garcia Arencibia M, Vetrini F, Erdin S, Erdin SU, Huynh T, Medina D, Colella P *et al* (2011) TFEB links autophagy to lysosomal biogenesis. *Science* 332: 1429–1433
- Martina JA, Chen Y, Gucek M, Puertollano R (2012) mTORC1 functions as a transcriptional regulator of autophagy by preventing nuclear transport of TFEB. *Autophagy* 8: 903–914
- Roczniak-Ferguson A, Petit CS, Froehlich F, Qian S, Ky J, Angarola B, Walther TC, Ferguson SM (2012) The transcription factor TFEB links mTORC1 signaling to transcriptional control of lysosome homeostasis. *Sci Signal* 5: ra42
- Medina DL, Di Paola S, Peluso I, Armani A, De Stefani D, Venditti R, Montefusco S, Scotto-Rosato A, Prezioso C, Forrester A *et al* (2015) Lysosomal calcium signalling regulates autophagy through calcineurin and TFEB. *Nat Cell Biol* 17: 288–299
- Ferron M, Settembre C, Shimazu J, Lacombe J, Kato S, Rawlings DJ, Ballabio A, Karsenty G (2013) A RANKL-PKCβ-TFEB signaling cascade is necessary for lysosomal biogenesis in osteoclasts. *Genes Dev* 27: 955–969
- Li Y, Xu M, Ding X, Yan C, Song Z, Chen L, Huang X, Wang X, Jian Y, Tang G *et al* (2016) Protein kinase C controls lysosome biogenesis independently of mTORC1. *Nat Cell Biol* 18: 1065–1077
- Palmieri M, Pal R, Nelvagal HR, Lotfi P, Stinnett GR, Seymour ML, Chaudhury A, Bajaj L, Bondar VV, Bremner L *et al* (2017) mTORC1-independent TFEB activation via Akt inhibition promotes cellular clearance in neurodegenerative storage diseases. *Nat Commun* 8: 14338
- Bao J, Zheng L, Zhang Q, Li X, Zhang X, Li Z, Bai X, Zhang Z, Huo W, Zhao X *et al* (2016) Deacetylation of TFEB promotes fibrillar Aβ degradation by upregulating lysosomal biogenesis in microglia. *Protein Cell* 7: 417–433
- Lin SY, Li TY, Liu Q, Zhang C, Li X, Chen Y, Zhang SM, Lian G, Liu Q, Ruan K *et al* (2012) GSK3-TIP60-ULK1 signaling pathway links growth factor deprivation to autophagy. *Science* 336: 477–481
- Yi C, Ma M, Ran L, Zheng J, Tong J, Zhu J, Ma C, Sun Y, Zhang S, Feng W *et al* (2012) Function and molecular mechanism of acetylation in autophagy regulation. *Science* 336: 474–477

14. Huang R, Xu Y, Wan W, Shou X, Qian J, You Z, Liu B, Chang C, Zhou T, Lippincott-Schwartz J *et al* (2015) Deacetylation of nuclear LC3 drives autophagy initiation under starvation. *Mol Cell* 57: 456–466
15. Su H, Yang F, Wang Q, Shen Q, Huang J, Peng C, Zhang Y, Wan W, Wong CCL, Sun Q *et al* (2017) VPS34 acetylation controls its lipid kinase activity and the initiation of canonical and non-canonical autophagy. *Mol Cell* 67: 907–921
16. Zhang J, Wang J, Zhou Z, Park JE, Wang L, Wu S, Sun X, Lu L, Wang T, Lin Q *et al* (2018) Importance of TFEB acetylation in control of its transcriptional activity and lysosomal function in response to histone deacetylase inhibitors. *Autophagy* 14: 1043–1059
17. Brownell JE, Zhou J, Ranalli T, Kobayashi R, Edmondson DG, Roth SY, Allis CD (1996) Tetrahymena histone acetyltransferase A: a homolog to yeast Gcn5p linking histone acetylation to gene activation. *Cell* 84: 843–851
18. Nagy Z, Tora L (2007) Distinct GCN5/PCAF-containing complexes function as co-activators and are involved in transcription factor and global histone acetylation. *Oncogene* 26: 5341–5357
19. Lerin C, Rodgers JT, Kalume DE, Kim SH, Pandey A, Puigserver P (2006) GCN5 acetyltransferase complex controls glucose metabolism through transcriptional repression of PGC-1 $\alpha$ . *Cell Metab* 3: 429–438
20. Wiper-Bergeron N, Salem HA, Tomlinson JJ, Wu D, Hache RJ (2007) Glucocorticoid-stimulated preadipocyte differentiation is mediated through acetylation of C/EBP $\beta$  by GCN5. *Proc Natl Acad Sci USA* 104: 2703–2708
21. Bararia D, Kwok HS, Welner RS, Numata A, Sarosi MB, Yang H, Wee S, Tschuri S, Ray D, Weigert O *et al* (2016) Acetylation of C/EBP $\alpha$  inhibits its granulopoietic function. *Nat Commun* 7: 10968
22. Sakai M, Tujimura-Hayakawa T, Yagi T, Yano H, Mitsushima M, Unoki-Kubota H, Kaburagi Y, Inoue H, Kido Y, Kasuga M *et al* (2016) The GCN5-CITED2-PKA signalling module controls hepatic glucose metabolism through a cAMP-induced substrate switch. *Nat Commun* 7: 13147
23. Chen L, Wei T, Si X, Wang Q, Li Y, Leng Y, Deng A, Chen J, Wang G, Zhu S *et al* (2013) Lysine acetyltransferase GCN5 potentiates the growth of non-small cell lung cancer via promotion of E2F1, cyclin D1, and cyclin E1 expression. *J Biol Chem* 288: 14510–14521
24. He H, Wang J, Liu T (2017) UV-Induced RPA1 acetylation promotes nucleotide excision repair. *Cell Rep* 20: 2010–2025
25. Jeitany M, Bakhos-Douaihy D, Silvestre DC, Pineda JR, Ugolin N, Moussa A, Gauthier LR, Busso D, Junier MP, Chneiweiss H *et al* (2017) Opposite effects of GCN5 and PCAF knockdowns on the alternative mechanism of telomere maintenance. *Oncotarget* 8: 26269–26280
26. Gerhart-Hines Z, Rodgers JT, Bare O, Lerin C, Kim SH, Mostoslavsky R, Alt FW, Wu Z, Puigserver P (2007) Metabolic control of muscle mitochondrial function and fatty acid oxidation through SIRT1/PGC-1 $\alpha$ . *EMBO J* 26: 1913–1923
27. Wellen KE, Hatzivassiliou G, Sachdeva UM, Bui TV, Cross JR, Thompson CB (2009) ATP-citrate lyase links cellular metabolism to histone acetylation. *Science* 324: 1076–1080
28. Lee Y, Dominy JE, Choi YJ, Jurczak M, Tolliday N, Camporez JP, Chim H, Lim JH, Ruan HB, Yang X *et al* (2014) Cyclin D1-Cdk4 controls glucose metabolism independently of cell cycle progression. *Nature* 510: 547–551
29. Tavares CD, Sharabi K, Dominy JE, Lee Y, Isasa M, Orozco JM, Jedrychowski MP, Kamenecka TM, Griffin PR, Gygi SP *et al* (2016) The methionine transamination pathway controls hepatic glucose metabolism through regulation of the GCN5 acetyltransferase and the PGC-1 $\alpha$  transcriptional coactivator. *J Biol Chem* 291: 10635–10645
30. Coste A, Louet JF, Lagouge M, Lerin C, Antal MC, Meziane H, Schoonjans K, Puigserver P, O'Malley BW, Auwerx J (2008), Vol. 105, pp 17187–17192
31. Tanner KG, Trievel RC, Kuo MH, Howard RM, Berger SL, Allis CD, Marmorstein R, Denu JM (1999) Catalytic mechanism and function of invariant glutamic acid 173 from the histone acetyltransferase GCN5 transcriptional coactivator. *J Biol Chem* 274: 18157–18160
32. Mao X, Gluck N, Li D, Maine GN, Li H, Zaidi IW, Repaka A, Mayo MW, Burstein E (2009) GCN5 is a required cofactor for a ubiquitin ligase that targets NF-kappaB/RelA. *Genes Dev* 23: 849–861
33. Pampliega O, Orhon I, Patel B, Sridhar S, Diaz-Carretero A, Beau I, Codogno P, Satir BH, Satir P, Cuervo AM (2013) Functional interaction between autophagy and ciliogenesis. *Nature* 502: 194–200
34. Shang Y, Wang H, Jia P, Zhao H, Liu C, Liu W, Song Z, Xu Z, Yang L, Wang Y *et al* (2016) Autophagy regulates spermatid differentiation via degradation of PDLIM1. *Autophagy* 12: 1575–1592
35. Smith ER, Belote JM, Schiltz RL, Yang XJ, Moore PA, Berger SL, Nakatani Y, Allis CD (1998) Cloning of *Drosophila* GCN5: conserved features among metazoan GCN5 family members. *Nucleic Acids Res* 26: 2948–2954
36. Scott RC, Schuldiner O, Neufeld TP (2004) Role and regulation of starvation-induced autophagy in the *Drosophila* fat body. *Dev Cell* 7: 167–178
37. Hallsson JH, Hafliadottir BS, Stivers C, Odenwald W, Arnheiter H, Pignoni F, Steingrimsson E (2004) The basic helix-loop-helix leucine zipper transcription factor Mitf is conserved in *Drosophila* and functions in eye development. *Genetics* 167: 233–241
38. Paolinelli R, Mendoza-Maldonado R, Cereseto A, Giacca M (2009) Acetylation by GCN5 regulates CDC6 phosphorylation in the S phase of the cell cycle. *Nat Struct Mol Biol* 16: 412–420
39. Fisher DE, Carr CS, Parent LA, Sharp PA (1991) TFEB has DNA-binding and oligomerization properties of a unique helix-loop-helix/leucine-zipper family. *Genes Dev* 5: 2342–2352
40. Muhle-Goll C, Gibson T, Schuck P, Schubert D, Nalis D, Nilges M, Pastore A (1994) The dimerization stability of the HLH-LZ transcription protein family is modulated by the leucine zippers: a CD and NMR study of TFEB and c-Myc. *Biochemistry* 33: 11296–11306
41. Hallsson JH, Hafliadottir BS, Schepsky A, Arnheiter H, Steingrimsson E (2007) Evolutionary sequence comparison of the Mitf gene reveals novel conserved domains. *Pigment Cell Res* 20: 185–200
42. Puertollano R, Ferguson SM, Brugarolas J, Ballabio A (2018) The complex relationship between TFEB transcription factor phosphorylation and subcellular localization. *EMBO J* 37: e98804
43. Bouche V, Espinosa AP, Leone L, Sardiello M, Ballabio A, Botas J (2016) *Drosophila* Mitf regulates the V-ATPase and the lysosomal-autophagic pathway. *Autophagy* 12: 484–498
44. Tognon E, Kobia F, Busi I, Fumagalli A, De Masi F, Vaccari T (2016) Control of lysosomal biogenesis and Notch-dependent tissue patterning by components of the TFEB-V-ATPase axis in *Drosophila melanogaster*. *Autophagy* 12: 499–514
45. Jackson GR, Wiedau-Pazos M, Sang TK, Wagle N, Brown CA, Massachi S, Geschwind DH (2002) Human wild-type tau interacts with wingless pathway components and produces neurofibrillary pathology in *Drosophila*. *Neuron* 34: 509–519
46. Chatterjee S, Sang TK, Lawless GM, Jackson GR (2009) Dissociation of tau toxicity and phosphorylation: role of GSK-3 $\beta$ , MARK and Cdk5 in a *Drosophila* model. *Hum Mol Genet* 18: 164–177
47. Polito VA, Li H, Martini-Stoica H, Wang B, Yang L, Xu Y, Swartzlander DB, Palmieri M, di Ronza A, Lee VM *et al* (2014) Selective clearance of



- aberrant tau proteins and rescue of neurotoxicity by transcription factor EB. *EMBO Mol Med* 6: 1142–1160
48. Sha Y, Rao L, Settembre C, Ballabio A, Eissa NT (2017) STUB1 regulates TFEB-induced autophagy-lysosome pathway. *EMBO J* 36: 2544–2552
  49. Stringer KF, Ingles CJ, Greenblatt J (1990) Direct and selective binding of an acidic transcriptional activation domain to the TATA-box factor TFIID. *Nature* 345: 783–786
  50. Sato S, Roberts K, Gambino G, Cook A, Kouzarides T, Goding CR (1997) CBP/p300 as a co-factor for the Microphthalmia transcription factor. *Oncogene* 14: 3083–3092
  51. Shin HJ, Kim H, Oh S, Lee JG, Kee M, Ko HJ, Kweon MN, Won KJ, Baek SH (2016) AMPK-SKP2-CARM1 signalling cascade in transcriptional regulation of autophagy. *Nature* 534: 553–557
  52. Zhang X, Shu L, Hosoi H, Murti KG, Houghton PJ (2002) Predominant nuclear localization of mammalian target of rapamycin in normal and malignant cells in culture. *J Biol Chem* 277: 28127–28134
  53. Rosner M, Hengstschlager M (2008) Cytoplasmic and nuclear distribution of the protein complexes mTORC1 and mTORC2: rapamycin triggers dephosphorylation and delocalization of the mTORC2 components rictor and sin1. *Hum Mol Genet* 17: 2934–2948
  54. Wan W, You Z, Xu Y, Zhou L, Guan Z, Peng C, Wong CCL, Su H, Zhou T, Xia H et al (2017) mTORC1 phosphorylates acetyltransferase p300 to regulate autophagy and lipogenesis. *Mol Cell* 68: 323–335 e6
  55. Napolitano G, Esposito A, Choi H, Matarese M, Benedetti V, Di Malta C, Monfregola J, Medina DL, Lippincott-Schwartz J, Ballabio A (2018) mTOR-dependent phosphorylation controls TFEB nuclear export. *Nat Commun* 9: 3312
  56. Li Q, Gong Z (2015) Cold-sensing regulates *Drosophila* growth through insulin-producing cells. *Nat Commun* 6: 10083
  57. Liu T, Wang Q, Li W, Mao F, Yue S, Liu S, Liu X, Xiao S, Xia L (2017) Gcn5 determines the fate of *Drosophila* germline stem cells through degradation of Cyclin A. *FASEB J* 31: 2185–2194
  58. Frenkel-Pinter M, Tal S, Scherzer-Attali R, Abu-Hussien M, Alyagor I, Eisenbaum T, Gazit E, Segal D (2016) Naphthoquinone-tryptophan hybrid inhibits aggregation of the tau-derived peptide PHF6 and reduces neurotoxicity. *J Alzheimers Dis* 51: 165–178
  59. Khurana V, Elson-Schwab I, Fulga TA, Sharp KA, Loewen CA, Mulkearns E, Tyynela J, Scherzer CR, Feany MB (2010) Lysosomal dysfunction promotes cleavage and neurotoxicity of tau *in vivo*. *PLoS Genet* 6: e1001026
  60. Chauhan S, Goodwin JG, Chauhan S, Manyam G, Wang J, Kamat AM, Boyd DD (2013) ZKSCAN3 is a master transcriptional repressor of autophagy. *Mol Cell* 50: 16–28
  61. Settembre C, De Cegli R, Mansueto G, Saha PK, Vetrini F, Visvikis O, Huynh T, Carissimo A, Palmer D, Klisch TJ et al (2013) TFEB controls cellular lipid metabolism through a starvation-induced autoregulatory loop. *Nat Cell Biol* 15: 647–658



**License:** This is an open access article under the terms of the Creative Commons Attribution-NonCommercial-NoDerivs 4.0 License, which permits use and distribution in any medium, provided the original work is properly cited, the use is non-commercial and no modifications or adaptations are made.